Applied Ocean Research 154 (2025) 104398

Contents lists available at ScienceDirect

Applied Ocean Research

journal homepage: www.elsevier.com/locate/apor

Research paper

Development of an acoustic sensor to monitor synthetic mooring lines

Martin Träsch [a,*], Peter Davies [a], Damien Le Vour'ch [a], Vincent Perier [a], Michel Répécaud [a], Guillaume Damblans [b], Romain Ribault [b], Jean Sebastien Verjut [b]

[a] Ifremer, Research and Technological Development Unit, 29280 Plouzané, France
[b] France Energies Marines, 29280 Plouzané, France

ARTICLE INFO

Keywords:
Mooring line
Acoustic altimeter
Floating offshore wind turbine
Synthetic ropes
Field measurement
Strain sensor
Dynamic stiffness

ABSTRACT

Fiber ropes (polyester, nylon, HMPE, etc.) are being considered for Floating Offshore Wind Turbines mooring lines, as they can reduce mooring weight and cost. Measuring the strain of these synthetic mooring lines could help to understand their behavior and long term monitoring of these systems could lead to their design and maintenance optimization.

A new strain sensor for synthetic mooring lines is proposed in this paper. It uses an ultrasonic altimeter to measure the distance between the transducer and a target fixed on a synthetic mooring line. This instrument is non-intrusive and can be fixed on anchor lines after their installation at sea. The measurement principle and prototype design are presented. Then, the validation of the concept in a water tank is described, demonstrating the feasibility of measuring length using acoustic waves with a high degree of accuracy. The acoustic strain sensor was deployed in operational condition on a demonstrator buoy mooring line in the Mediterranean sea, together with a wire displacement sensor and a load sensor. The measurements from these three instruments are compared, showing the ability of the acoustic sensor to monitor the behavior of a mooring line at sea.

1. Introduction

Offshore Renewable Energies represent a huge worldwide potential. Among the available technologies, the development of offshore wind energy, and in particular floating wind turbines, is set to be a major challenge in the years ahead in order to achieve the energy transition objectives.

For Floating Wind Turbines, hybrid mooring lines combining chain and fiber ropes (polyester, nylon, HMPE, etc.) are often considered as they can reduce the weight and the cost of the mooring compared to typical steel chain line (Weller, 2015). They can also benefit from better durability and lower sensitivity to fatigue, corrosion, torsion, and out-of-plane loads and their viscous behavior can reduce peak loads. Indeed, textile mooring lines experience highly non-linear behavior, including visco-elasticity, hysteresis (Weller et al., 2014b), creep (Civier et al., 2022), ageing (Weller et al., 2014a) and fatigue (Chevillotte et al., 2020).

There is a need to be able to measure the tension and elongation of textile anchor lines in order to understand their behavior and monitor these systems over the long term (up to 30 years). It is essential to follow changes in their properties with respect to load history and seawater ageing. However, there is still a lack of data on the dynamic behavior of synthetic mooring lines at sea. Therefore, mooring systems are often over-sized, resulting in significant cost increases, especially when designed in accordance with current oil industry standards (Anon, 2021). By optimizing the design of textile mooring lines, by reducing their diameter for example, production costs can be reduced. This is a major issue for offshore renewable energy (Anon, 2011). Monitoring data of mooring lines in service would also be useful to validate numerical models for the design of floating offshore wind turbine mooring lines (Pham et al., 2019a), to predict the remaining service life and to organize maintenance operations (Pham et al., 2019b). Several authors have studied damage development in synthetic ropes, for example (Beltran et al., 2017; Lian et al., 2022, 2023).

There are many ways of monitoring the condition and behavior of textile anchor lines. Current practices and standards recommend visual inspections, counting the number of cycles, and replacing ropes that have been subject to more than 70% of the maximum break strength (Anon, 2013, 2005, 2015). However, field inspection solely by visual methods is insufficient because the visibility can be altered by sediment and fouling, and also because many offshore ropes are based on load-bearing cores inside a cover and deteriorate internally (Rebel et al., 2000). Indeed, internal damage, mainly caused by internal abrasion, governs the lifetime of ropes and can modify their mechanical properties (Davies et al., 2013).

* Corresponding author.
E-mail address: martin.trasch@ifremer.fr (M. Träsch).

https://doi.org/10.1016/j.apor.2024.104398
Received 23 February 2024; Received in revised form 9 December 2024; Accepted 23 December 2024
Available online 8 January 2025

The floater position and motion can easily be monitored, which can give insight on the load history of the lines, but this is not sufficient to provide information on the mooring line state and behavior without significant modeling. Strain gauges, instrumented shackles or load cells can also give valuable information on the tension in the mooring lines and can be complementary to other monitoring systems. They can be placed inline, during the installation of the floating system, when they could be damaged, or after the installation, in by-pass, by taking up the tension of the mooring line, which requires careful handling.

Among the technologies proposed to monitor fiber ropes as reviewed by Laura (1995), Rebel et al. (2000) and Oland et al. (2020), many require the presence of an embedded materiel inserted in the rope during its fabrication, especially those using conductivity (Schmieder et al., 2015), magnetism (Huntley et al., 2015), thermography (De Angelis, 2002) or optical fiber (O'Hear, 2003) (Gordelier et al., 2020). The risk with these is that the presence of the measuring device can affect the response. Other methods can be impacted by the presence of biofouling or by damping from surrounding water, such as those based on vibration (Kwun and Burkhardt, 1991; Williams et al., 1984). Sensors using a spring and extension system linked to a position sensor to measure the local length or width of a rope element (Ilaka and Zerza, 2014) could lack reliability or robustness, and can also be affected by biofouling.

Acoustic-ultrasonic systems using transmitter and receiver fixed on the rope have already been proposed and tested in the laboratory ((Williams et al., 1984; Ferreira et al., 2000; Padilla et al., 0000)). These systems monitor acoustic wave propagation through the rope, and could detect its flaws or even assess its mechanical properties łand how they change during fatigue. However, to the authors knowledge, none have been successfully tested at sea.

The basic idea behind the monitoring system presented here is to adapt the use of an ultrasonic altimeter. This system has been adapted to measure the distance between a transducer and a target fixed on a synthetic mooring line. This enables the elongation of the line to be measured, and therefore to monitor tensile fatigue and peak strain. It has been patented under n° WO2024017612. It can be adapted to any moored system such as a wind turbine, an aquaculture cage, an oceanographic buoy,. . . ,Among the main advantages of this instrument is that it is simple, robust, non-intrusive and can be fixed on anchor lines after their installation at sea.

However, the axial strain is the only dimension measured, and the measurement is local. For example it would be insufficient to detect cut or pulled strand, compression damage, local creep, abrasion or melted fibers located elsewhere on the rope (Oland et al., 2020). Therefore, other monitoring systems would be needed.

It would be very useful combined with other information (float position and motion, load, visual inspection, etc.) and especially with a preliminary characterization of the mechanical properties of the rope, combined with modeling of its behavior (Pham et al., 2019b).

First, the operating principle of the sensor and the characteristics of the first prototype are described. Then the validation of the concept is presented, first in the laboratory, demonstrating the feasibility of measuring length using acoustic waves with a high degree of accuracy. This step was carried out in a seawater tank. Several tests were carried out in order to assess the sensibility results to the angle and salinity. Then, the set-up for the first operation of this system at sea is described. It consisted of testing a line with known characteristics under a significant load that varied over time, in a sheltered sea environment on the Sainte Anne du Portzic test platform. The final section presents the installation of the acoustic strain sensor in operational conditions at the Mistral open sea test site, currently home to the Monabiop buoy of the Monamoor project piloted by France Energies Marines. The acoustic strain sensor was installed on one of the three mooring lines, together with a wire displacement sensor and a load sensor. The measurements from these three instruments are then compared.

2. Presentation of the sensor

2.1. Measurement principle

This paper presents the development of an underwater sensor able to measure the elongation of textile mooring lines. It consists of an adaptation for mooring lines of the working principle of an acoustic altimeter. It uses an acoustic transducer fixed at one point of the line and a target used as an acoustic mirror at another point a few meters away (Fig. 1). By measuring the time between the emission of the beam and its reflection, the system provides the distance between both points. The relative variation of this distance is the elongation of the monitored portion of the line.

2.2. Prototype design

The acoustic strain sensor prototype is a modified application of the Altus sensor which is an acoustic altimeter for observing sediment dynamics, developed by NKE Instrumentation in partnership with Ifremer (Jestin et al., 1998). According to the manufacturer, this sensor emits an acoustic beam at frequency of 2 MHz, with an opening of 3.6° at −3 dB, then measures the return time and the back-scatter amplitude. It can measure a distance from 200 to 2000 mm with a resolution of 0.41 mm and an accuracy of ±5 mm. Their system also includes a pressure transducer with a range of 0 to 20 m, an accuracy of ±6 cm and a resolution of 0.8 cm. The sampling rate is adjustable from 0.5 s to 99 h. The memory card size is 4 Mo, which is equivalent to 10^6 measurements. The internal clock deviation is noted to be less than 1 min/month

Each measurement comprises 5 cycles, each consisting of an acoustic pulse (time of ping 0.0125 ms) followed by a listening period of the back-scattered signal of 9 ms. The first cycle consists of measuring the maximum intensity of the back-scattered signal in the environment. It is followed by 4 cycles of distance measurement conditioned by exceeding a previously configured back-scattered intensity threshold. This comes from the original application of the sensor to distinguish different types of sediment. In our application, only one distance measurement with one threshold is recorded in order to use less memory.

One of the main limitations of the sensor is that the celerity value required to calculate distance is a constant, set by the manufacturer. However, this value may vary in the environment, leading to significant measurement uncertainty, as discussed below.

Two frames have been designed in polyoxymethylene to host the altimeter and the 300 mm diameter target with a cylindrical clamping system (Fig. 2). They can be adapted to and installed on existing mooring lines without generating high stress concentrations that could damage them. The frames can be easily handled and installed by divers, so that they can also change the sensors or retrieve data.

In some of the following experiments (Section 3), two Altus systems are used in order to have a redundancy of the measurement. For other tests (Section 4), they are deployed along with a temperature gauge to assess the speed of the sound in the local seawater.

3. Qualification of the method

3.1. Calibration in seawater tank

Two ALTUS altimeters were mounted on their frame, which enabled them to be fixed to a steel tube. The target was fixed to the same tube, at a distance controlled by stainless steel standard tubes of lengths known to a $1/10th$ mm (see Fig. 3). Four distances were tested: 2000 mm, 1500 mm, 1000 mm, 500 mm. The tests were repeated in three tanks filled with water of different salinity (seawater, brackish water and freshwater). Tank dimensions were 3 m by 1.5 m with water depth of 0.5 m. For each measurement, the acquisition time was set at 1 min and the sampling frequency at 2 Hz. Salinity and temperature

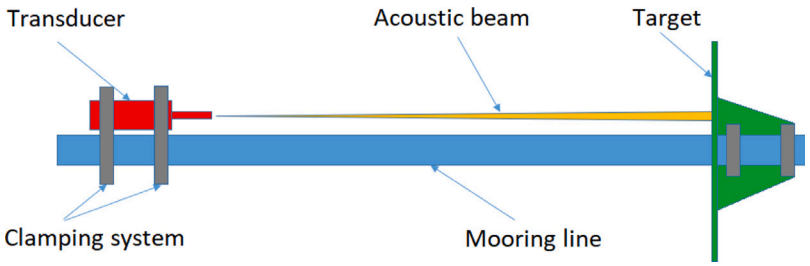

Fig. 1. Schematic diagram of the acoustic strain sensor working principle.

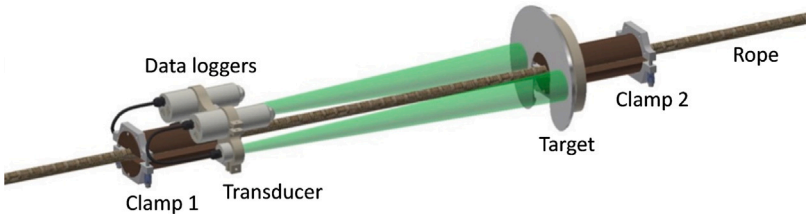

Fig. 2. 3D picture of the first acoustic strain sensor prototype.

Fig. 3. Pictures of the sensors being tested in a seawater tank.

were measured at the beginning and end of each series of measurements using a calibrated Tetracon sensor No. 300232/24407 (Table 1).

The sound celerity considered by ALTUS altimeters is a fixed value. However, the water temperature and salinity have a significant influence on the sound celerity in the water, therefore, the results were corrected here using the Mackenzie formulation (Eq. (1)), where T is the temperature in degrees Celsius, S the salinity in PSU and z the depth in meters. a_i are non-dimensional constants with the following values: $a_1 = 1448.96$; $a_2 = 4.591$; $a_3 = -5.304 \times 10^{-2}$; $a_4 = 2.374 \times 10^{-4}$; $a_5 = 1.34$; $a_6 = 1.63 \times 10^{-2}$; $a_7 = 1.675 \times 10^{-7}$; $a_8 = -1.025 \times 10^{-2}$; $a_9 = -7.139 \times 10^{-13}$;

$$C = a_1 + a_2T + a_3T^2 + a_4T^3 + a_5(S-35) + a_6z + a_7z^2 + a_8T(S-35) + a_9Tz^3 \quad (1)$$

Fig. 4 presents the results of the tank calibration before and after the correction using Mackenzie formula (here z = 0.1 m is considered). After the correction, maximum measurement error is 0.4%, while the maximum standard deviation is 0.44 mm. The results presented here show that particular attention should be paid to adjusting the speed of sound in the altimeter. Considering seawater at 15 °C and 34 PSU at 10 m below the surface, 0.21% celerity variation is caused by 1 °C difference, 0.08% for 1 PSU and 0.01% for 1 m.

The amplitude threshold of the backscattered signal can be adjusted for distance detection. The maximum distance difference observed between the minimum threshold (10% of the maximum echo) and the maximum (90% of the maximum echo) was less than 1.17 mm. This demonstrates the sensitivity of the results to the threshold amplitude of the backscattered signal. In the following experiments, a threshold of 70% of the maximum echo has been used.

The study of the influence of the distance from the target on the intensity of the signal echo led to the observation of a significant drop in the average intensity (25% of the maximum echo) for the longest distance of approximately 2 m. Below this distance, the echo intensity varies between 65 and 85% for distances of 1500 mm to 500 mm.

Specific tank tests were carried out to estimate the influence of the orientation of the transducers on the intensity of the backscattered signal. Fig. 5 clearly shows an attenuation of the backscattered signal proportional to the angle of impact of the acoustic beam on the target. It can be seen that for an orientation of 10° of the beams on the target, the maximum echo is less than 20% of the intensity of the transmitted signal and that at 15°, the signal is zero.

Deploying the two sensors simultaneously and then alternately did not reveal any interference between the two transducers.

These tests show that the system can measure distance with a maximum error of around 0.4% and standard deviation of about 4 mm in a seawater tank. The range of operation of the system should be from 500 mm to 2000 mm, with an angle less than +/- 10°. To compensate for bias due to temperature variations, it may be useful to use a temperature sensor with the same recording frequency as the altimeter.

3.2. Quayside experiment : comparison with a wire transducer and a load sensor

The quayside experiment involved fixing the altimeter and the target on either side of an elastic rope. This assembly was attached to a ballast through a SF1 load cell from NKE. The other end was connected to a rope that can be pulled from the top of the quay using a hoist

Table 1
Measured temperature and salinity, and calculated celerity for each test case.

Case	Temperature (°C)	Salinity (PSU)	Celerity (m/s)
Seawater, altimeter 1	13.8	34.0	1501.6
Seawater, altimeter 2	14.5	34.1	1504.0
Brackish water, altimeter 1	16.8	18.3	1492.7
Brackish water, altimeter 2	18.5	18.5	1498.3
Freshwater, altimeter 1	14.5	0.0	1463.5
Freshwater, altimeter 2	15.2	0.0	1465.9

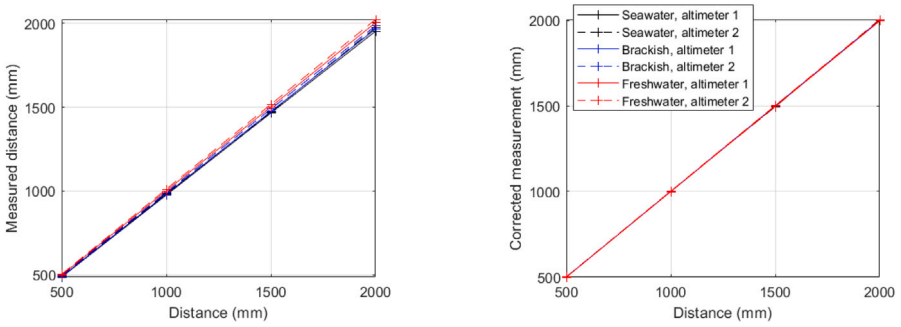

(a) Before celerity correction (b) After celerity correction

Fig. 4. Results of the calibration in tank tests before and after the celerity correction.

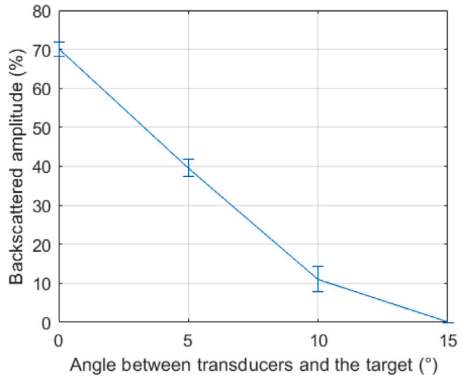

Fig. 5. Influence of the angle of the target on the backscatter amplitude in tank test. Standard deviations are presented as errorbars.

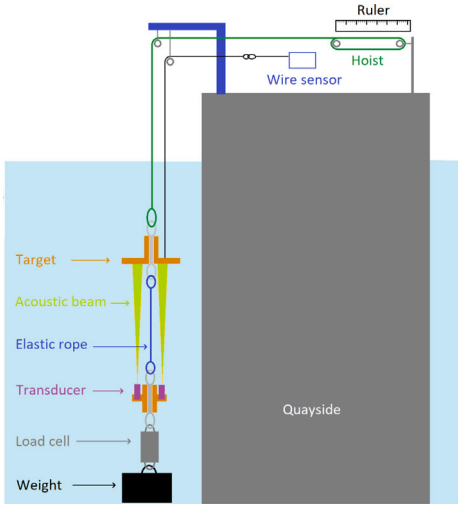

Fig. 6. Diagram of the experimental set-up.

attached to a gallows with a pulley. The set up is completed by a wire sensor DVT-250-A from PSI-TRONIX and by visual measurements using a ruler (see Fig. 6). The mechanical behavior of the elastic rope had first been characterized on a tension test bench.

For practical reasons, the first measurement is taken with the maximum extension of the elastic rope enabled by the set-up. The tension is then gradually released, in steps of 10 cm, until the only tension in the elastic is the target's weight. The rope is then pulled up in 10 cm increments back to the initial position.

The ruler measurement results are consistent with the other results. They deviate linearly with tension because of the elasticity of the rope in the hoist. They also have a significant measurement uncertainty, of the order of a few millimeters. They will therefore not be used to analyze the results.

The altimeter data corresponding to a maximum echo $\leq 20\%$ are considered outliers and replaced by the average between the data at 1 s interval. The distance is corrected using Mackenzie's formula, assuming a temperature of $T = 16.4$ °C, a salinity $S = 34.78$ PSU measured by the nearby COAST-HF Marel Iroise databuoy (Rimmelin-Maury et al., 2023) and z, the average depth between the transducer and the target over the test duration. A celerity of $c = 1512.6$ m/s is obtained, compared with 1468.7 m/s and 1479.7 m/s programmed in the altimeters.

The mean and standard deviation of the distance are calculated over 30 s for the altimeter. The first measurement is taken as the reference and subtracted from all the values for both sensors.

The maximum distance measurement difference with the wire sensor was respectively 7.9 mm and 16.6 mm for altimeter 1 and 2. The greatest difference is obtained for the measurement point where the elastic is least stretched, where the target could oscillate more easily under the effect of the waves. However, as the wire sensor measurement is obtained visually on a voltmeter, the risk of error is greater. Fig. 7 also shows that the standard deviation of the acoustic measurement is greater when the elastic is relaxed.

There is a small difference in distance measured by the two Altus sensors, which increases according to the distance measured. This could be caused by the target being tilted relative to the altimeters when the tension is applied to the system. In particular, the end of the wire

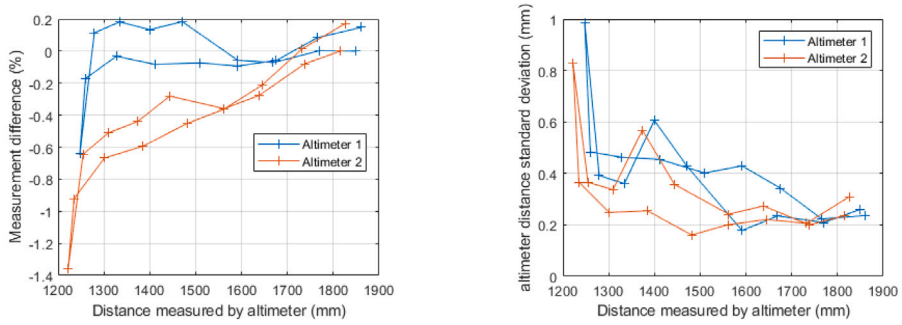

(a) Relative difference between the wire and the acoustic sensors measurement

(b) Standard deviation of the acoustic altimeter mesurements

Fig. 7. Results of the quayside experiments.

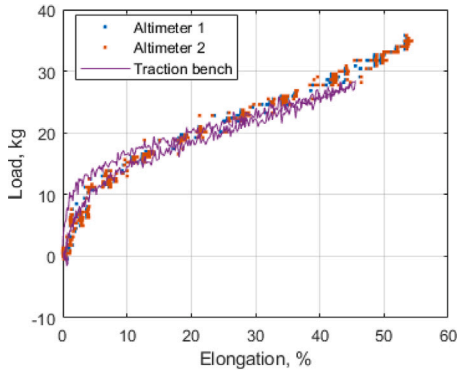

Fig. 8. Load–strain diagram obtained by the quayside experiment and by the laboratory test bench.

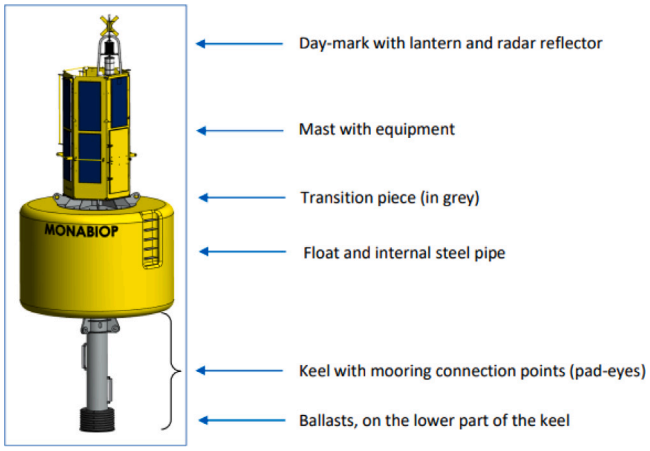

Fig. 9. Description of the Monabiop buoy.

sensor was fixed to the side of the target corresponding to the altimeter 1, which may explain its better results. In a similar case in a real application, it would then be necessary to average the results of the two altimeters to determine the distance. Indeed, if the target is not perpendicular to the beam, the distance to the center of the target should be the average of the two measurements.

The relative difference is less than 1.5%. If only the closest altimeter to the wire sensor is considered, and only the points where the elastic is under tension, the deviation is less than 0.2%. The standard deviation of the Altus measurements over 30 s, presented in Fig. 7, is less than 1 mm. If we consider only the points when the rope is in tension, this value drops to 0.6 mm.

The elongation is given by the formula: (L-min(L))/min(L); considering that the smallest length measured by the Altus corresponds to the resting length of the elastic. Fig. 8 shows the stress in the elastic as a function of elongation for the quayside experiment with four strands, and for the measurements in the laboratory on the test bench on a single strand multiplied by four. There is a good agreement between the two curves, with small differences that might be caused by the different limit conditions. This demonstrates that the mechanical behavior of an elastic mooring line could be accurately monitored with the proposed acoustic sensor system.

4. Validation on the monabiop buoy

4.1. Deployment

The acoustic sensor has been deployed under operating condition at sea on the Monabiop buoy (see Fig. 9) as part of the Monamoor Project (MONitoring of polyAmide MOORing lines) led by France Energies Marines and Ifremer (Anon, 2024).

The buoy was deployed on February 18th 2023 at the Mistral offshore test site, at approximate position 43° 18.93' N 4° 54.94' E, with a water depth of 57 m. It is 10.0 m high, weighs 7 t, has a diameter of 3.7 m and a draft of 4.5 m.

The buoy is moored to three 20t deadweight anchors placed at 200 m (for 0° N and 240° WSW lines) and 260 m (for the 120° ESE line) from the buoy. Lines 1 (N) and 2 (WSW) are made of both polyamide and chain segments while line 3 (ESE) is only made of chain (see Table 2). The sensors used in this study are placed on line 2. They are listed below.

The Altus altimeter used to build the acoustic strain sensor prototype is an autonomous sensor. During this deployment, it was programmed to make 10-min-long acquisitions at a sampling rate of 2 Hz, separated by 1-hour pauses.

A Wisens TD autonomous temperature and pressure sensor from NKE was deployed alongside to correct for sound velocity. The manufacturer guarantees a resolution of 0.001 °C and an accuracy of 0.005 °C.

A wire displacement transducer was installed on the same clamp as the acoustic strain sensor (specially designed and built to fit the 40 mm diameter rope). It consists of a stainless steel wire connected to an elastic line to keep it taut. The stainless steel wire drives a revolution-counting pulley. A similar device was successfully used previously during a campaign to qualify polyester mooring lines on a floating offshore oil & gas exploration rig off West Africa (Foulhoux et al., 1999). The two measuring systems were clamped to the top of the mooring line just below the upper spliced region (Fig. 10).

The clamp system is fitted with tightening screws so that the transducer can be mounted on a mooring line by divers. These screws are

Table 2
Mooring lines composition.

Component	line 1 (m)	line 2 (m)	line 3 (m)	Diameter (mm)	Weight (kg/m)
Upper chain	3	3	4	45	39.8
Upper Nylon	20	20	–	40	1
Main chain	110	110	110	38	28.4
Lower Nylon	40	100	–	40	1
Lower Chain	35	35	100	38	28.4

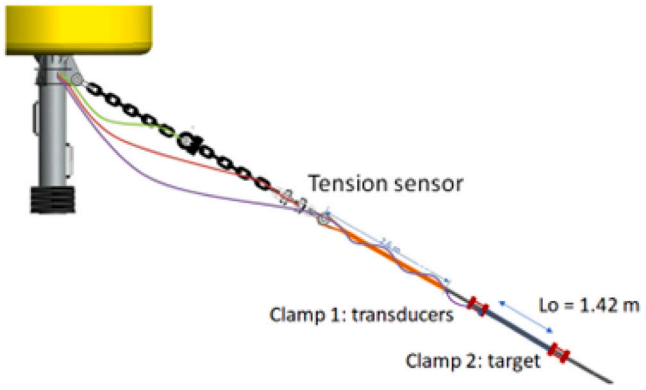

Fig. 10. Position of transducers on mooring line.

Fig. 11. Detail of clamping system.

spring loaded in order to maintain the pressure on the rope if its diameter reduces, Fig. 11.

This system has been used in several previous campaigns, both on land on test machines and at sea, and we have not seen any sign of clamp slip. It is also easy to mark the rope around the clamp position so that any movement can be detected.

The other measurement used here comes from a load cell from Garos with a capacity of 200 kN. These two sensors are connected to a Dewesoft Krypton data acquisition unit that records all the other measurements from the Monabiop buoy anchors at a frequency of 10 Hz, so that they are all synchronized together.

These sensors were first calibrated and mounted on a full size rope sample for testing on a 20 t mechanical test bench before deployment on the Monabiop buoy. Calibration factors are 100 mm/V for the wire transducer and 40 kN/V for the load cell. The data acquisition unit's range is set to ±5 V with a 24-bit resolution.

Both strain sensors were installed on the Monabiop buoy on 21st March 2023. The acoustic strain sensor was recovered on 7th July 2023, with its memory full. Data are available up to 28th April 2023 ($\approx 10^6$ acquisitions). A time drift of +6s was noted between deployment and recovery on the acoustic strain sensor. Fig. 12 shows the prototype as installed during the deployment.

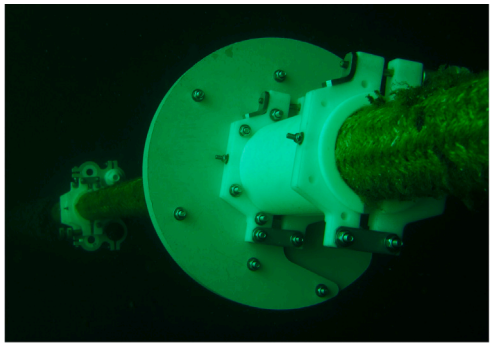

Fig. 12. Image of the acoustic strain sensor prototype following deployments.

A second deployment occurred from 21th July 2023 to 18th September 2023. However, the Dewesoft acquisition system for the wire and load sensors stopped working from the 26th July, and the altimeter presented a low back-scatter amplitude from 18th to 27th July, with low quality results, leaving only 10 days of usable data. That is why the results from this second deployment are not presented further in this paper.

Fig. 13 presents the metocean conditions during the first deployment: the wave measured by a Datawell DWR MkIII wave buoy at position 43° 12.500' N, 05° 13.800' E near Le Planier island are shown in Fig. 13(a) and the wind measured on the nearby Mesurho buoy in Fig. 13(b).

4.2. Data process

Fig. 14 shows the raw data of distance and maximum backscattered amplitude of the acoustic sensor. It initially assumes a sound speed of 1479.66 m/s. Its results were corrected by a celerity value calculated using Mackenzie's formula (equation (1)) from temperature and pressure measurements taken by the Wisens TD probe near the altimeter and by the salinity value measured by Mesurho 20 m below the surface (43° 19.2 N, 4° 52 E), at a distance of around 5 km from the buoy towards the mouth of the Rhône (Pairaud et al., 2016). The results are considered valid when the measured distance is between 1420 mm and 1470 mm.

Raw results from the wire sensor show significant drift. They are therefore processed by subtracting a moving average over 60 s, and replacing the outliers (defined as $\Delta x > 20$ mm) and the surrounding values over ±30 s by the last valid value.

Fig. 15 shows the three processed signals (from acoustic sensor, wire sensor and force sensor) that are synchronized and compared in the following. A visual comparison shows similar variations over the duration of the measurements, although there are some notable differences.

As only the variation of the line's length is studied here, a 1-minute moving average high-pass filter is applied on both elongation signals. Then, an inter-correlation is calculated using Matlab's *xcorr* function between each 10-minute window of the acoustic sensor and the corresponding signal on the wire sensor (equation (4), where * is the complex conjugate, c is the standardized correlation coefficient and N is the sample size). The maximum correlation coefficient (Fig. 16) and

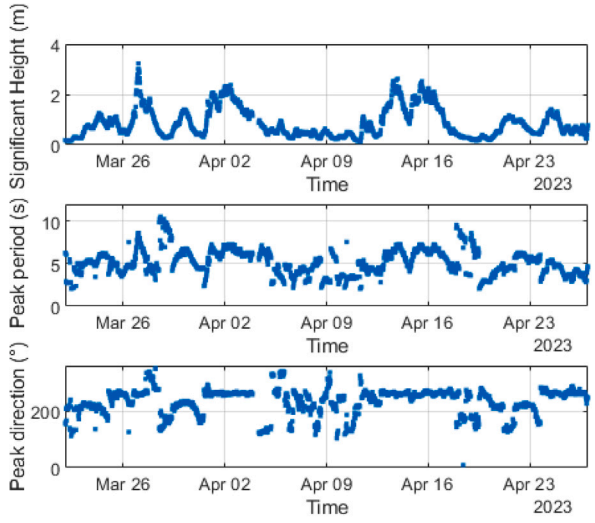

(a) Wave measured by Candhis station 01305

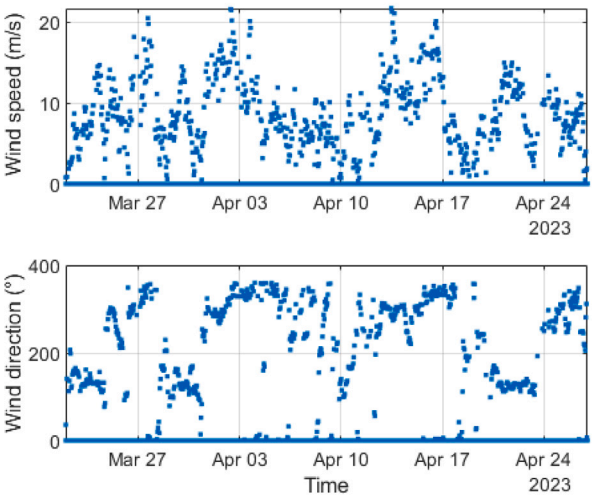

(b) Wind measured on COAST-HF Mesurho

Fig. 13. Meocean conditions during first deployment.

the matching offset are considered to synchronize each window. Only samples with a correlation coefficient greater than 0.8 are considered hereafter.

$$c(m) = \frac{\hat{R}_{xy}(m-N)}{\sqrt{\hat{R}_{xx}(0)\hat{R}_{yy}(0)}} \tag{2}$$

$$\hat{R}_{xy}(m, m>0) = \sum_{n=0}^{N-m-1} x_{n+m} y_n^* \tag{3}$$

$$\hat{R}_{xy}(m, m<0) = \hat{R}_{xy}(-m) \tag{4}$$

Fig. 17 shows a superposition of the elongation signals measured by both sensors over three-minute windows, corresponding to two different sea states: $H_{m0} = 1.16$ m; $T_p = 6.1$ s; $D_w = 262°$; $V = 10.4$ m/s; D_v=330° for Fig. 17(a) and $H_{m0} = 0.91$ m; $T_p = 4.7$ s; $D_w = 215°$; $V = 11.6$ m/s; $D_v = 134°$ for Fig. 17(b). The main difference is the wind direction that is aligned with the mooring line in the second case.

The results are very good in both cases. The wire sensor has a better spatial and temporal resolution. However, it can only be used to compare length variations as its drift requires its average value to be subtracted.

Peaks from the acoustic sensor are larger than from the wire sensor, especially for high elongation amplitude. These peaks match measurement points where the intensity of the back-scattered acoustic signal is particularly low (see Fig. 18). They are therefore considered unreliable. This could be due to the large amount of particles in the water coming from the nearby Rhone river. Furthermore, the acoustic sensor uses a fixed amplitude threshold instead of a peak detection method to detect the target's distance, which could also induce some small errors in a dynamic environment.

However, there are also some periods of low backscatter amplitude and low quality of signal during the second leg that are not linked with the highest amplitudes. They could also be due to a significant amount of sediments in the water column, or to the presence of biofouling.

4.3. Sensor comparison

To compare the results from the different sensors, a simple linear regression was then performed: coefficients β_0 and β_1 are determined to find $\hat{y}$ the approximate value of y as a function of x (Eqs. (5) & (6)). The coefficient of determination R^2 is calculated by Eq. (7), with $\bar{y}$ the mean of y.

$$\hat{y} = \beta_0 + \beta_1 x \tag{5}$$

$$\begin{bmatrix}\beta_0\\ \beta_1\end{bmatrix} = \begin{bmatrix}1 & y_1\\ 1 & y_2\\ \vdots & \\ 1 & y_N\end{bmatrix}^{-1}\begin{bmatrix}x_1\\ x_2\\ \vdots\\ x_N\end{bmatrix} \tag{6}$$

$$R^2 = 1 - \frac{\sum_{i=1}^{N}(y_i - \hat{y}_i)^2}{\sum_{i=1}^{N}(y_i - \bar{y})^2} \tag{7}$$

Fig. 19 shows a point cloud comparison of measurements from the acoustic sensor with the wire sensor over 10-minute windows corresponding to the same times as in Fig. 17, while Fig. 20 shows the same type of results but comparing the elongation sensors with the load measurement.

The better resolution of the wire sensor and the aberrant spikes at the high limit of the acoustic sensor's measurement can also be noticed here. The scatter of the results is relatively low, which confirms the confidence we can have in the measurement.

Fig. 21 shows the results of linear regression on all the measurements considered to be valid. There are relatively large variations (+/-20%) in the directional coefficients involving the acoustic sensor until the beginning of April. These could be linked to variations in local salinity that have not been measured, and that generate changes in the celerity of sound that have not been properly taken into account. There is an anomaly around the first of April, which coincides with a period of weak echoes (see Fig. 18). There are also a few peaks in the directional coefficients of the wire sensor, that are certainly linked to the pre-processing of the data to remove the drift. The coefficients of determination R^2 fluctuate around 0.9. They are very similar for the three sensors.

Assuming the mooring line to be viscoelastic (equation (8)), the linear regression between the load F (kN) and the elongation $x = L - L_0$ (mm) can be used to assess its mechanical properties: the stiffness E (kN/mm) and the viscosity ν (kN/mm s).

$$F = Ex + \nu\frac{dx}{dt} \tag{8}$$

As the reference length L_0 of the line segment under consideration is unknown, it is estimated as the sum of the acoustic sensor corrected distance average and the y-intercept of the regression between the acoustic sensor and the load sensor: $L_0 = \bar{L} + \bar{\beta}_0$. This gives $L_0 = 1424$ mm.

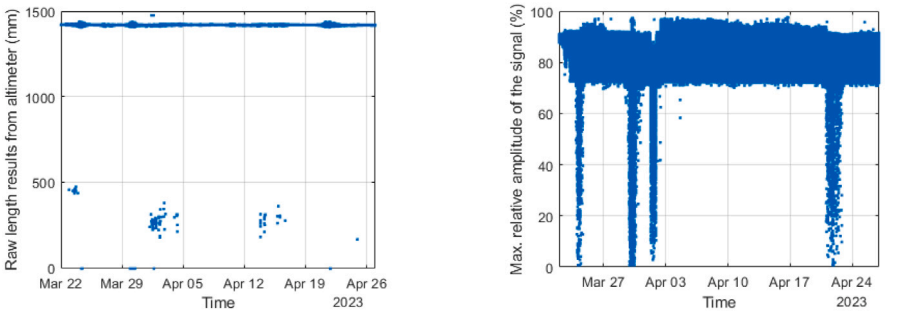

(a) Raw measured length (b) Max. amplitude of backscattered signal

Fig. 14. Raw results from the acoustic sensor during 1st deployment on Monabiop buoy.

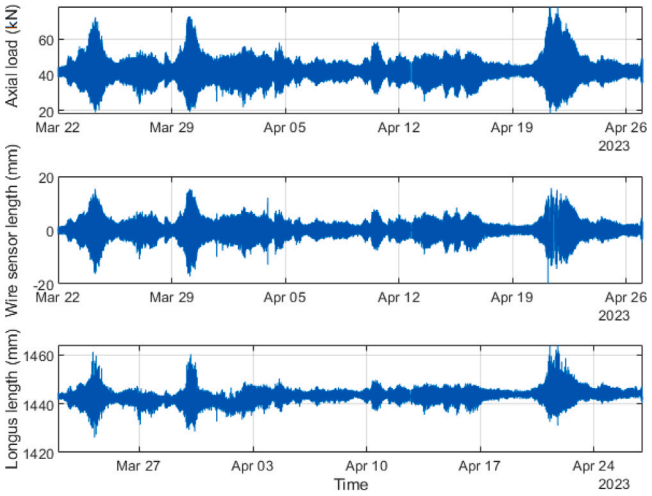

Fig. 15. Axial load, length from wire sensor and length from acoustic sensor during the first deployment.

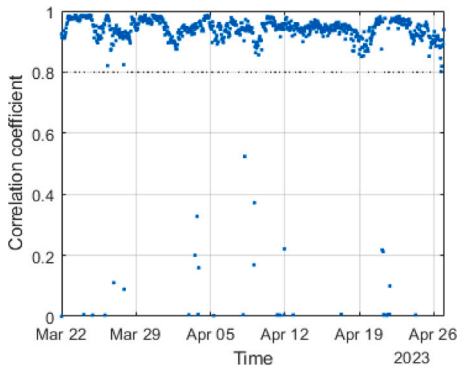

Fig. 16. Normalized correlation coefficient between the length variation signals from the wire and acoustic sensors.

However, the reference load depends on the load history (Civier et al., 2022). In our case, the maximum load experienced by the rope is about 30% of the Maximum Break Load, so the expected residual strain is about 5%, according to laboratory tests on a sample of this rope.

The strain $\sigma = x/L_0$, and the relative stiffness E^*(kN/%)= $\frac{100E}{L_0} = \frac{L_0}{100\beta_1}$ can then be calculated. The estimated stiffness is shown in Fig. 22 for both transducers. The values agree well from 4th April 2023. The value oscillates around 27 kN/%. A trend can be noticed depending on the load amplitude range, that explains some of the variations in the estimated stiffness.

Bench tests had previously been carried out on a wet, unaged, full-scale rope sample after bedin to 250kN (the rope was preloaded to stabilize properties). Dynamic load tests with a period of 20 s and an amplitude of 10 kN around 42 kN (i.e. 15% of the MBL) gave a dynamic stiffness of 16.65 kN% (Fig. 23 & Fig. 24). Dynamic stiffness was defined as the linear regression between all the force and strain data-points recorded during the last five cycles at each load level. The same sample was then dried and tested with the same conditions, resulting in 21.55 kN/% dynamic stiffness. There is therefore a significant difference between the bench tests and the sea trials. The reasons for these differences will have to be investigated in further research. This clearly shows the importance of carrying out measurements not just in the laboratory but in real conditions at sea, and of having suitable sensors for this purpose.

5. Uncertainty analysis

To estimate the degree of confidence that can be placed in the results, an uncertainty analysis was carried out. The distance is obtained from the return time of the backscattered signal using equation (9). It is then corrected for variations in celerity.

$$L_{raw} = (T_{backscatttering})/2 * c_{sensor} \tag{9}$$

$$L_{estimated} = L_{raw} c_{estimated} / c_{sensor} \tag{10}$$

Two applications will be considered. First, the measurement uncertainty will be calculated for the calibration experiment in a seawater tank. The expanded measurement uncertainty is given by Eq. (11) with $k = 2$ the expansion factor.

$$U_{measurement} = k\sqrt{U^2_{sensor} + U^2_{experiment}} \tag{11}$$

The uncertainty associated with the sensor characteristics can be estimated from the manufacturer's technical datasheet (equation (12)). The sensor linearity and clock drift are considered not significant. This results in $U_{sensor} = 2.89$ mm for the 2 meters standard length.

$$U_{sensor} = \sqrt{U^2_{resolution} + U^2_{accuracy}} \tag{12}$$

- $U_{resolution} = \frac{resolution}{2\sqrt{3}} = \frac{0.41}{2\sqrt{3}} = 0.12$ mm
- $U_{accuracy} = \frac{accuracy}{\sqrt{3}} = \frac{5}{\sqrt{3}} = 2.89$ mm

The uncertainty associated with the experimental calibration method is assessed by taking into account the uncertainty of the standard tube length $U_{reference}$, the uncertainty associated with sound celerity variations $U_{celerity}$ and the uncertainty of the linear regression $U_{regression}$ (equation (13)).

$$U_{calibration} = \sqrt{U^2_{reference} + U^2_{regression} + U^2_{celerite}} \tag{13}$$

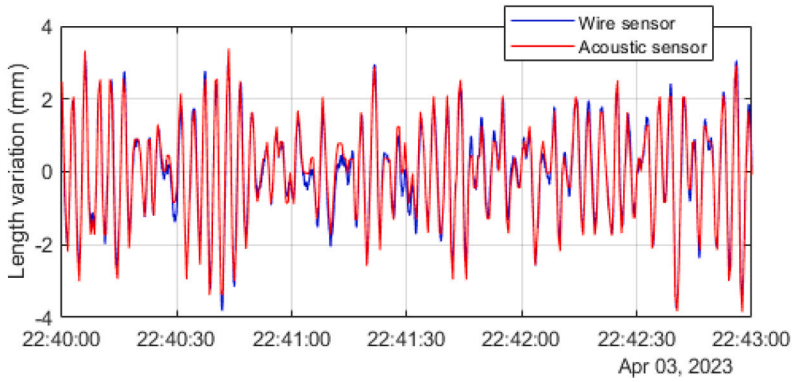

(a) Over a period of low strain variation

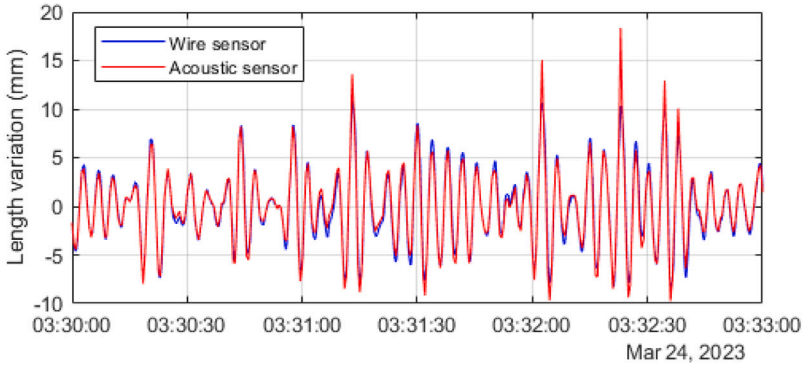

(b) Over a period of high strain variation

Fig. 17. Examples of synchronization of wire and acoustic sensor signals over 3 min.

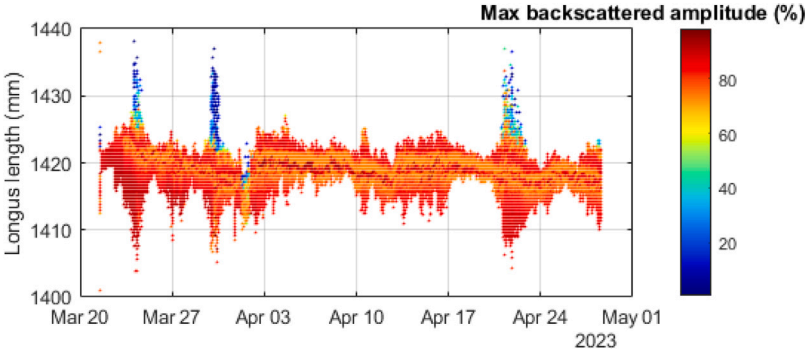

Fig. 18. Target distance influence on the backscattered amplitude.

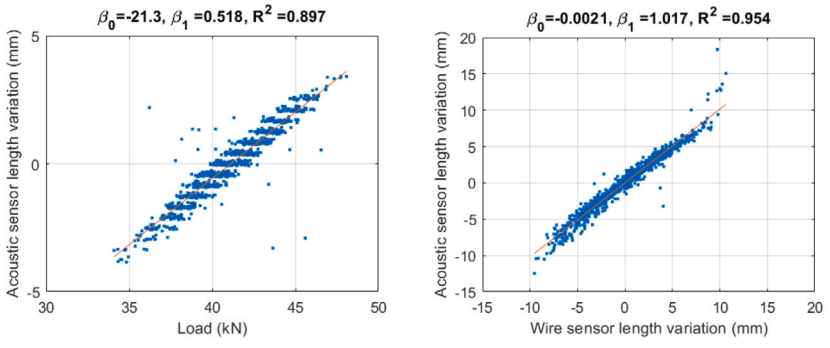

(a) Over a period of low strain variation (b) Over a period of high strain variation

Fig. 19. Scatter diagrams of elongation measurements by wire sensor compared to acoustic sensor measurements.

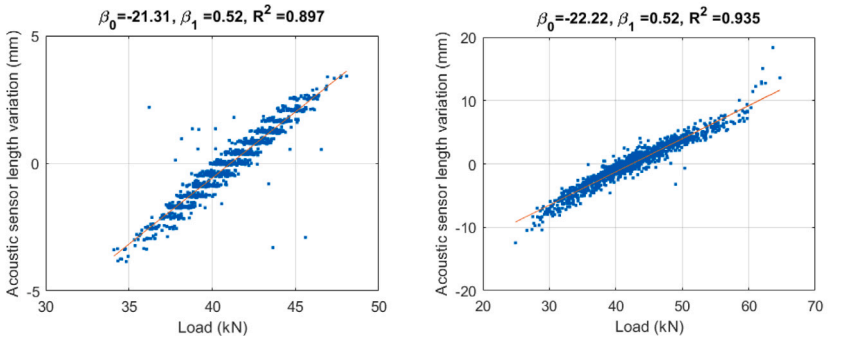

(a) Over a period of low strain variation (b) Over a period of high strain variation

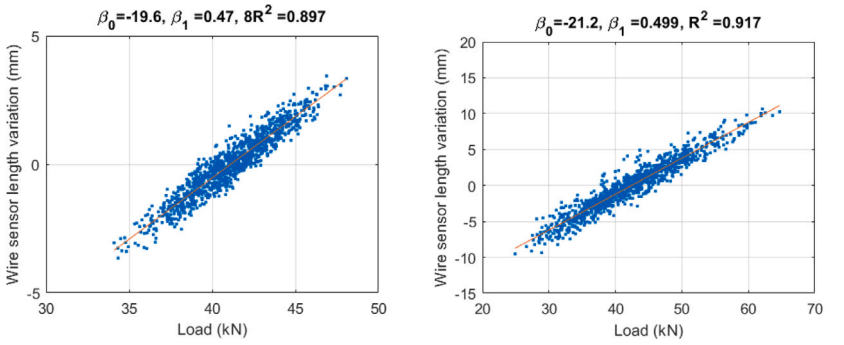

(c) Over a period of low strain variation (d) Over a period of high strain variation

Fig. 20. Scatter diagrams of elongation measurements by acoustic sensor (a-b) and wire sensor (c-d) as a function of tension measurement.

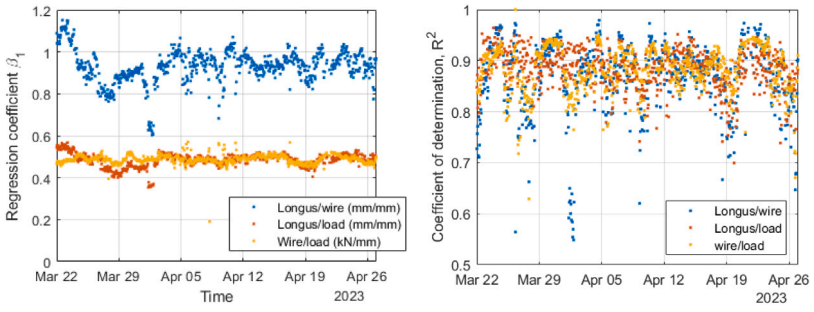

(a) Directional coefficient β_1 (b) Coefficient of determination R^2

Fig. 21. Results of linear regression between the three sensors results.

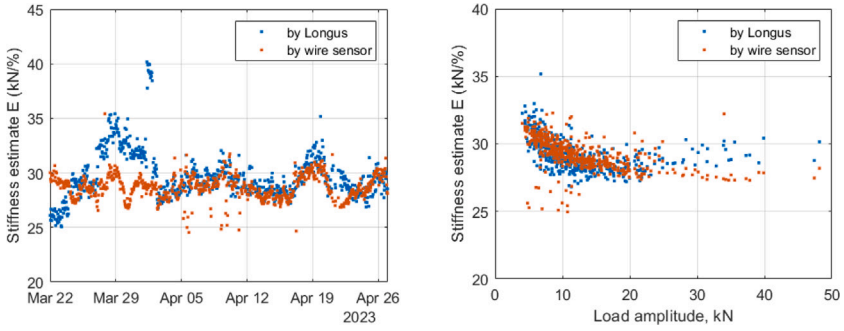

Fig. 22. Estimation of stiffness by the acoustic sensor and the wire sensor: (a) as a function of time and (b) as a function of load amplitude, from 4 April 2023.

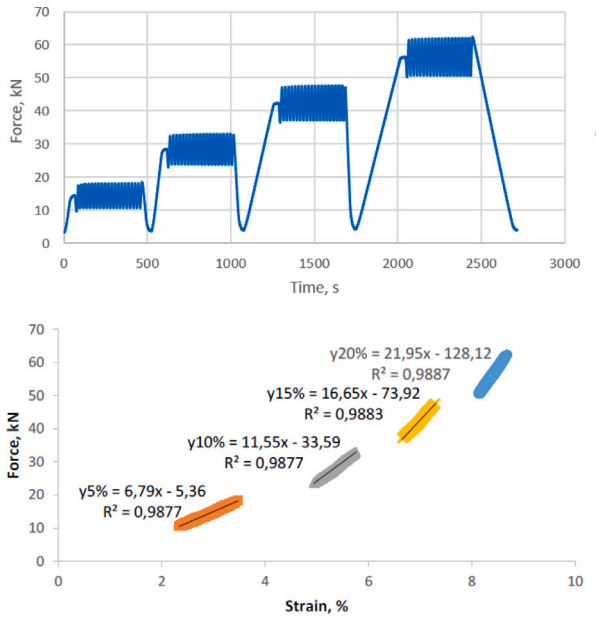

Fig. 23. (a) Load versus time and (b) stiffness measurements on wet bedded-in rope during laboratory tests.

- $U_{reference} = \frac{U_{standardlength}}{\sqrt{3}} = \frac{0.1}{\sqrt{3}} = 0.06$ mm
- $U_{celerity} = \frac{L(c_{max}) - L(c_{min})}{2\sqrt{3}} = \frac{2007.53 - 2004.18}{2\sqrt{3}} = 0.97$ mm. It is calculated from max and min calculated celerity values during the experiment, with the addition of uncertainties from temperature and salinity gauge and Mackenzie's formula: $c_{max} = 1504.66$ m/s and $c_{max} = 1502.14$ m/s.
- $U_{regression} = 0.35$ mm is the standard deviation of residual errors between the regression slope and the measurements points.

This results in $U_{calibration} = 1.03$ mm. The total measurement uncertainty in the seawater tank is then $U_{measurement} = 6.14$ mm, or 0.31% of measured length. In this calculation, the uncertainty associated with the angle between the target and the transducer is considered not to be significant, nor is the one associated with the backscatter amplitude threshold as it was programmed at the maximum possible value (see Fig. 24).

The same process can be applied for the deployment on the Monamoor buoy, with equation (14).

$$U_{Monamoor} = \sqrt{U_{celerity}^2 + U_{threshold}^2 + U_{target\_angle}^2} \quad (14)$$

- $U_{celerity} = \frac{L(c_{max}) - L(c_{min})}{2\sqrt{3}} = \frac{1414.2 - 1393.7}{2\sqrt{3}} = 5.94$ mm. Here, the salinity measured near the surface by Mesurho is considered, as it varies much more, from 20 PSU to 38.35 PSU (Fig. 25) during the experiment, resulting in a possible celerity variation from 1482.05 to 1507.6 m/s.
- $U_{threshold} = \frac{0.83}{2\sqrt{3}} = 0.24$ mm. In order to register as many data as possible, a threshold of 10% has been used during this deployment. To assess the linked uncertainty, the max. error measured by tuning this parameter in the tank experiment is considered (1.17 mm) and then multiplied the length ratio 1.42 m /2 m.
- $U_{angle} = \frac{2.09}{\sqrt{3}} = 1.21$ mm. Assuming the max angle variation is ±1° and a distance of 120 mm between the transducer and the line central axis, a distance deviation of $\pm 120 sin(1°) = 2.09$ mm is obtained.

The value of $U_{Monamoor} = 6.05$ mm is obtained, which leads to a $U_{measurement}$ of 12.14 mm, or 0.85% of the measured length.

The measurement uncertainty analysis shows that the accuracy of the results could be greatly improved by selecting a more suitable sensor, and a more accurate determination of the speed of sound, either by direct measurement or by measuring the local salinity along with the depth and temperature.

6. Conclusion and perspectives

The development of an autonomous strain sensor for synthetic mooring lines has been presented. A prototype using an existing acoustic altimeter has been designed. It was first tested in a seawater tank, then in a quayside experiment, which demonstrated the feasibility of the concept.

Other tests have been performed that were not presented here in order to keep this paper concise: a test on an elastic line under a parachute lifting bag that exerted a varying force depending on the tidal level at the Ste-Anne-du-Portzic test site; and a test on a 76 mm diameter nylon rope of one of the WaveGem station mooring lines at the SEMREV test site (SEM-REV, 2019).

The deployment on the Monabiop mooring line, together with a wire displacement sensor and a load sensor, showed that the acoustic strain sensor can be used in operational conditions. The comparison of the data from two sensors used to measure the elongation of a textile line, after filtering and synchronization, enabled a validation of their results, particularly with regard to strain variations. An assessment of the dynamic stiffness was also performed with a good agreement between the two sensors.

The resolution of the wire transducer is better, but it experienced a very high drift over a shorter lifetime. Indeed, the wire transducer lacked robustness. At the end of the second leg, it was entangled and perturbed by heavily biofouling colonization. Furthermore, the acquisition of the wire transducer and load cell stopped at the beginning of the second leg due to acquisition system damage.

The acoustic sensor also showed drift, but to a much lesser extent. This could be caused in part by the variation in the celerity of sound in seawater, the estimation of which could have been improved by a local measurement of salinity. The quality of the acoustic sensor measurements is lower for distances greater than 1450 mm, particularly the intensity of the backscattered signal. This could be due to the presence of large amount of sediment in the water, combined with a use of a fixed threshold peak detection.

The installation and recovery operations of the acoustic sensor were carried out as planned despite the constraints associated with an offshore site, so the final demonstration in a real-life situation was validated. This showed the value of an autonomous sensor, that can be deployed after the installation of a mooring line and that is robust and reliable. It is complementary to other sensors, and can help to monitor changes in mechanical properties of a synthetic line.

A future deployment could involve a shorter installation distance, of around 1 or 1.2 m for example. The synthetic fiber mooring lines we have studied to date are taut leg moorings so the line curvature is very low. The acoustic strain sensor should be suitable for taut and semi-taut mooring systems, with some limitations for catenary lines or lazy wave cables. The anticipated application cases focus on synthetic Nylon mooring lines, for which a permanent tension is recommended by the BV standard NI 432 (Anon, 2021).

For a more precise measurement system one could use two transducers, placed on each side of the line, which would help quantify and minimize potential errors due to the curvature of the line induced by waves or currents. Indeed, it would enable the difference between both measured lengths to be analyzed, instead of considering only one measurement. This would help to assess the inclination of the target relative to the transducers. Furthermore, by calculating the average

Fig. 24. Images of rope on laboratory test frame showing load sensor (middle) and wire transducer (right).

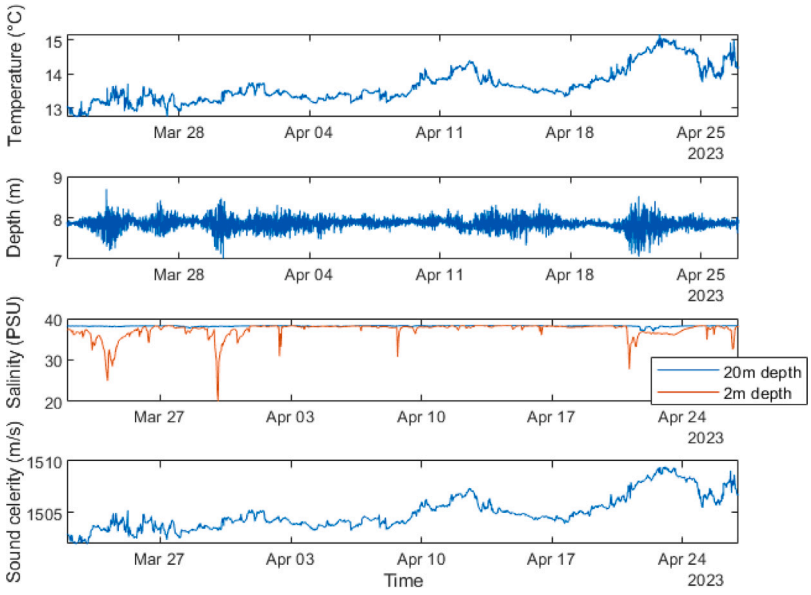

Fig. 25. Temperature and depth measurements from the Winsens TD, salinity from Mesurho station and estimated celerity during the deployment.

value of both measurements, one would minimize the error induced by the change of angle of the target.

The low resolution of the acoustic measurements could also penalize the results, so an improved version of the acoustic strain sensor prototype could use another acoustic source, in order to enhance the resolution, the sampling frequency, and benefit from a much larger autonomy. The lack of synchronization complicates post-calculation, but the system can also be adapted by changing the way it communicates, which could allow results to be obtained in real time or to be synchronized with other sensors.

CRediT authorship contribution statement

Martin Träsch: Writing – original draft, Visualization, Methodology, Investigation, Formal analysis, Data curation, Conceptualization. **Peter Davies:** Writing – review & editing, Validation, Supervision, Methodology, Conceptualization. **Damien Le Vour'ch:** Methodology, Conceptualization. **Vincent Perier:** Writing – original draft, Investigation. **Michel Répécaud:** Writing – review & editing, Supervision, Methodology, Conceptualization. **Guillaume Damblans:** Project administration, Methodology. **Romain Ribault:** Software, Methodology, Investigation. **Jean Sebastien Verjut:** Supervision, Project administration, Methodology.

Declaration of competing interest

The authors declare the following financial interests/personal relationships which may be considered as potential competing interests: Peter Davies reports financial support was provided by French National Research Agency. Michel Repecaud has patent #WO2024017612 issued to Ifremer. If there are other authors, they declare that they have no known competing financial interests or personal relationships that could have appeared to influence the work reported in this paper.

Acknowledgments

This work benefited from France Energies Marines and State financing managed by the National Research Agency under the Investments for the Future program bearing the reference ANR-10-IED-0006-32.

References

Anon, 2005. DNV-RP-E304. Damage assessment of fibre ropes for offshore moorings.
Anon, 2011. Accelerating Marine Energy: The Potential for Cost Reduction-Insights from the Carbon Trust marine energy accelerator. Technical Report, Carbon Trust.
Anon, 2013. DNV-OS-E303. Offshore fibre ropes.
Anon, 2015. DNV-RP-E305. Design, testing and analysis of offshore fiber ropes.
Anon, 2021. BV NR 493 Classification of mooring systems for permanent and mobile offshore units.

Anon, 2024. Projet Monamoor. France Energies Marines. https://www.france-energies-marines.org/projets/monamoor/. (Accessed: September 2024).
Beltran, J.F., Ramirez, N., Williamson, E., 2017. Simplified analysis of the influence of strain localization and asymmetric damage distribution on static damaged polyester rope behavior. Ocean Eng. 145, 237–249.
Chevillotte, Y., Marco, Y., Bles, G., Devos, K., Keryer, M., Arhant, M., Davies, P., 2020. Fatigue of improved polyamide mooring ropes for floating wind turbines. Ocean Eng. 199, 107011.
Civier, L., Chevillotte, Y., Bles, G., Montel, F., Davies, P., Marco, Y., 2022. Short and long term creep behaviour of polyamide ropes for mooring applications. Ocean Eng. 259, 111800.
Davies, P., Lacotte, N., Kibsgard, G., Craig, R., Cannell, D., François, S., Lodeho, O., Konate, K., Mills, S., François, M., 2013. Durability of fibre ropes for deep sea handling operations. In: 32nd International Conference on Ocean, Offshore and Arctic Engineering. OMAE2013.
De Angelis, C., 2002. Synthetic fiber cable with temperature sensor. US Patent 6392551 B2.
Ferreira, M., Lam, T.M., Koncar, V., Delvael, Y., 2000. Nondestructive testing of polyaramide cables by longitudinal wave propagation: Study of the dynamic modulus. Polym. Eng. Sci. 40 (7), 1628–1634.
Foulhoux, L., Pennec, S., Damy, G., Davies, P., 1999. Testing of a large diameter polyester rope offshore West Africa. In: Ninth International Offshore and Polar Engineering Conference, ISOPE-I-99-172. Brest, France, p. 337.
Gordelier, T., Thies, P.R., Rinaldi, G., Johanning, L., 2020. Investigating polymer fibre optics for condition monitoring of synthetic mooring lines. J. Mar. Sci. Eng. 8 (2), 103.
Huntley, E., Grabandt, O., Gaëtan, R., 2015. Non-Destructive Test methods for high-performance synthetic rope. In: Ridge, I.M.L. (Ed.), Proceedings of the 5th International OIPEEC Conference.
Ilaka, M., Zerza, H., 2014. Apparatus for recognizing the replacement state of a high-strength fiber rope for lifting gear. US Patent 0027401 A1.
Jestin, H., Bassoullet, B., Le Hir, P., L'Yavanc, J., Degres, Y., 1998. Development of ALTUS, a high frequency acoustic submersible recording altimeter to accurately monitor bed elevation and quantify deposition or erosion of sediments. In: IEEE Oceanic Engineering Society. OCEANS'98. Conference Proceedings. Nice, France.
Kwun, H., Burkhardt, G.L., 1991. Relationship between reflected signal amplitude and defect size in rope inspection using a transverse-impulse vibrational wave. NDT&E Int. 24 (6).
Laura, P.A.A., 1995. Evaluating the structural condition of synthetic and metallic cables. Ocean Eng. 22 (6), 551–562.
Lian, Y., Zhang, B., Ji, J., Pan, Z., Jiang, T., Zheng, J., Ma, G., Zhu, Z., Zhu, Z., Chen, W., 2023. Experimental investigation on service safety and reliability of full-scale HMPE fiber slings for offshore lifting operations. Ocean Eng. 285, 115447.
Lian, Y., Zhang, B., Zheng, J., Liu, H., Ma, G., Yim, S.C., Y., Zhao, 2022. An upper and lower bound method for evaluating residual strengths of polyester mooring ropes with artificial damage. Ocean Eng. 262, 112243.
O'Hear, N., 2003. Optical scanning apparatus for ropes nondestructive test monitoring system. In: Oceans 2003. Celebrating the Past ... Teaming Toward the Future (IEEE Cat. No.03CH37492), vol. 3, pp. 1335–1341 Vol.3.
Oland, E., Schlanbusch, R., Falconer, S., 2020. Condition monitoring technologies for synthetic fiber ropes - a review. Int. J. Prognostics Health Manag. 8 (2).
Padilla, L.S., Bull, P., Royer, R.L., Owens, S.E., 0000. Non-contact acoustic signal propagation property evaluation of synthetic fiber rope, US Patent 8.958.994 B2.
Pairaud, I., Répécaud, M., Ravel, C., Fuchs, R., Arnaud, M., Champelovier, A., Rabouille, C., Bombled, B., Toussaint, F., Garcia, F., Raimbault, P., Verney, R., Meule, S., Gaufres, P., Bonnat, A., Cadiou, J.-F., 2016. MesuRho. Plateforme instrumentée de suivi des paramètres environnementaux à l'embouchure du Rhône. In: Mesures à Haute Résolution Dans L'environnement Marin Côtier. CNRS Alpha. ISBN 978-2-271-08592-4. Boulogne-sur-Mer, pp. 73–87.
Pham, H.-D., Cartraud, P., Schoefs, F., Soulard, T., Berhault, C., 2019a. Dynamic modeling of nylon mooring lines for a floating wind turbine. Appl. Ocean Res. 87, 1–8.
Pham, Hong-Duc, Schoefs, Franck, Cartraud, Patrice, Soulard, Thomas, Pham, Hien-Hau, Berhault, Christian, 2019b. Methodology for modeling and service life monitoring of mooring lines of floating wind turbines. Ocean Eng. 193, 106603.
Rebel, G., Chaplin, C.R., Groves-Kirkby, C., Ridge, I.M.L., 2000. Condition monitoring techniques for fibre mooring ropes. Insight - J. Br. Inst. Non-Destr. Test. 42 (6).
Rimmelin-Maury, P., Charria, G., Répécaud, M., Quéméner, L., Beaumont, L., Guillot, A., Gautier, L., Prigent, S., Le Becque, T., Bihannic, I., Bonnat, A., Le Roux, J.-F., Grossteffan, E., Devesa, J., Bozec, Y., Gautier de Charnacé, C., 2023. COAST-HF-Marel-Iroise Buoy's Time Series (French Research Infrastructure ILICO) : Long-Term High-Frequency Monitoring of the Bay of Brest and Iroise Sea Hydrology. SEANOE.
Schmieder, A., Heinze, T., Michael, M., 2015. Failure Analysis of High-Strength Fiber Ropes. In: 20th Symposium on Composites. In: Materials Science Forum, vol. 825, Trans Tech Publications Ltd, pp. 891–898.
SEM-REV, 2019. Wavegem: the wave energy recovery prototype. https://sem-rev.ec-nantes.fr/english-version/devices-tested/wavegem%C2%AE-wave-energy-prototype. (Accessed on February, 2024).
Weller, S.D., 2015. Synthetic mooring ropes for marine renewable energy applications. Renew. Energy.
Weller, S.D., Davies, P., Vickers, A.W., Johanning, L., 2014a. Synthetic rope responses in the context of load history: Operational performance. Ocean Eng. 83, 111–124.
Weller, S.D., Davies, Peter, Vickers, A.W., Johanning, L., 2014b. Synthetic rope responses in the context of load history: Operational performance. Renew. Energyy 83, 111–124.
Williams, J.H., Hainsworth, J., Lee, S.S., 1984. Acoustic-ultrasonic nondestructive evaluation of double-braided nylon ropes using the stress wave factor. Fibre Sci. Technol. 21 (3), 169–180.